Discrete breathers and energy localization in a nonlinear honeycomb lattice

Yi Dai,[1] Hang Yu,[1] Zhigang Zhu,[2,1] Yisen Wang,[1,*] and Liang Huang[1]
[1]*Lanzhou Center for Theoretical Physics, Key Laboratory of Theoretical Physics of Gansu Province, and Key Laboratory for Magnetism and Magnetic Materials of MOE, Lanzhou University, Lanzhou, Gansu 730000, China*
[2]*Department of Physics, Lanzhou University of Technology, Lanzhou, Gansu 730000, China*

(Received 3 June 2021; accepted 17 November 2021; published 2 December 2021)

Discrete breathers (DBs) in nonlinear lattices have attracted much attention in the past decades. In this work, we focus on the formation of DBs and their induced energy localization in the nonlinear honeycomb lattice derived from graphene. The key step is to construct a reduced system (RS) with only a few degrees of freedom, which contains one central site and its three nearest neighbors. The fixed points and periodic orbits of the RS can be obtained from the Poincaré section of the dynamics. Our main finding is that the long-running DB solution of the full honeycomb system corresponds to the periodic orbit given by one of the fixed points of RS, where the central site and its nearest neighbors vibrate inversely. When the initial condition deviates from this fixed point, the local vibration is attracted to it after a short transient process. When the initial condition is assigned to other fixed points of the RS, the initial excitation energy flows to the other part of the full system quickly, resulting in a delocalized wave propagation. Another main finding is that the long-lived DB solutions emerge only when the initial excitation energy is larger than a threshold value, above which the frequency of the DB exceeds the phonon band edge. The excitation energy generally dissipates from the local region due to the interactions between the DB and phonons near the Γ point in the dispersion relation. These results provide a holistic physical picture for the DB solutions in two-dimensional nonlinear lattices with complex potentials, which will be crucial to the understanding of energy localization in the realistic two-dimensional materials.

DOI: 10.1103/PhysRevE.104.064201

I. INTRODUCTION

Discrete breathers (DBs), also known as intrinsic localized modes or nonlinear localized excitations, have been a central topic in nonlinear dynamics of anharmonic lattices with discrete translational symmetry, which have attracted much attention in the nonlinear dynamics community during the past decades [1–9]. The DBs can be defined as the time-periodic and spatially localized solutions of discrete systems, which have been rigorously proved in Fermi-Pasta-Ulam-Tsingou (FPUT) lattice [10], and Klein-Gordon lattice [11]. The DBs have also been found theoretically in various coupled ordinary differential equations of Hamiltonian systems [12–21]. Experimental observations of DBs have been reported with various physical systems [3,22–24], such as electrical lattice [25], forced-damped array of coupled pendulum [26], diatomic granular crystals [3], and $\mathcal{PT}$-symmetric nonlinear metamaterials [27].

Discreteness and nonlinearity are two key recipes for the emergence of DBs, where discreteness sets up the phonon band edges and nonlinearity can modulate the frequency of possible time-periodic excitations [28,29]. The frequency of the long-lived DB can be found beyond the band edge of the phonon band, where the localized wave packet will not be dispersed by the linear modes [7,30]. The DBs may have frequencies above or below the phonon band, which correspond to systems with hard-type or soft-type anharmonicity, respectively [7]. The latter case generally requires on-site term in the potential, which shifts the lower boundary of the band to a finite positive value. However, a recent work shows that the long-range interactions can also open a gap below the phonon band, and supports the existence of low-frequency DBs without on-site potential [31]. The existence of gap DBs, also referred to as intra-band DBs, needs the phonon band to have a gap between adjacent branches, which is generally the case for nonlinear diatomic lattices [15,32–34]. In addition, according to the Fourier spectrum of the trajectory, the DBs can be periodic, quasiperiodic, or chaotic [35,36].

Various methods have been developed to search the DB solutions in nonlinear lattices. The simplest way to observe the DB is to exploit the targeted initial condition, i.e., displace one or few sites to the target values, which, however, cannot obtain DB solutions within a reasonable precision [37]. Another approximate method widely used in the literature is the rotating wave approximation [38,39]. A method with higher precision is based on the correspondence between the DBs and the periodic orbits in the phase space or in the Fourier spectrum, which can be achieved with the iteration procedure of Newton and steepest descent scheme [29]. Here, the reduced problem scheme proposed by Flach and Willis [28,40,41] is employed, as the DB is highly spatially localized and pertains certain symmetries, and a two degree-of-freedom subsystem for a central site and its nearest neighbors is considered, while the other sites are assumed to remain static. The dynamical behavior for this subsystem can be obtained completely via the Poincaré sections. The stable fixed points on the Poincaré section correspond to periodic orbits of the original dynamics

*wys@lzu.edu.cn

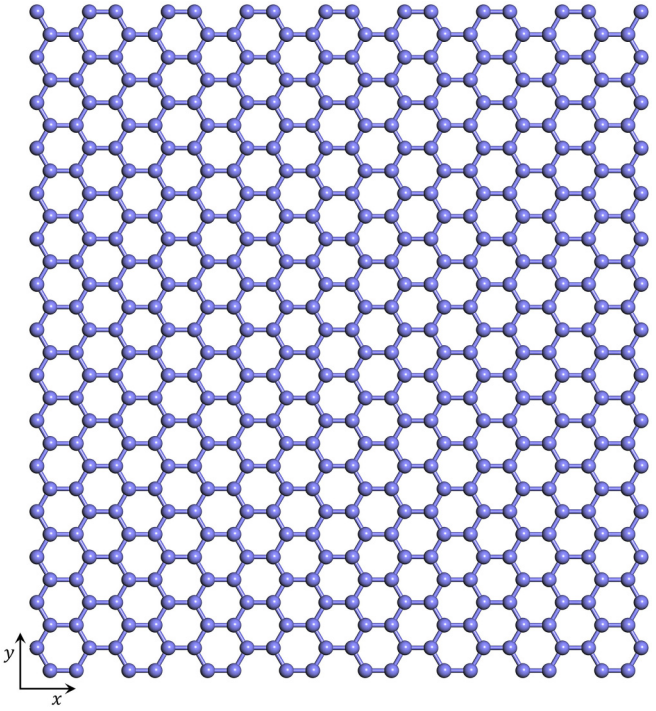

FIG. 1. Schematic of the nonlinear honeycomb lattice with a total of 480 sites. The full system used in the MD simulations contains 4800 sites in total, where the periodic boundary condition is applied along x and y axes.

for the subsystem, which lead to the DB solutions of the full system.

Graphene sheet, where carbon atoms are tightly packed in two-dimensional (2D) honeycomb lattice, supplies an outstanding system for the investigation of DBs [42–44]. The DBs in fully hydrogenated graphene, also termed as graphane, is confirmed with density functional theory [42] and molecular dynamics (MD) simulations [45], where a hydrogen atom oscillates with large amplitude in the direction normal to the graphene plane. To excite the gap DB, strain needs to be applied to the graphene sheet to open the gap of phonon band between the acoustic and optical branches [46–49]. The transverse DBs have also been investigated with MD simulations, where the initial condition is given by a bell-shaped function, and the MD simulations are performed by large-scale atomic/molecular massively parallel simulator (LAMMPS) software with the adaptive intermolecular reactive empirical bond-order (AIREBO) potential [44]. Besides that, the DBs also exist in the realistic model for carbon-hydrogen systems with tight-binding MD simulations [50].

In this paper, we would like to search the DB solutions in the nonlinear honeycomb lattice with the reduced problem scheme as many 2D natural and artificial materials have this structure. In Sec. II, the nonlinear honeycomb lattice, an abstract model of graphene lattice [51], is introduced, whose potential energy characterizing the interaction between adjacent sites is given by a simplified valence force field (VFF) model [52]. The reduced system (RS) is proposed in Sec. III, which contains only a few degree-of-freedom, i.e., a central site and its three nearest neighbors. In addition, when the three neighbors move synchronously, the RS can be further simplified as a two degree-of-freedom system, where a complete dynamical analysis can be performed, which may shed light on the search of DBs in the full system. In Sec. IV, numerous numerical simulations are performed with the simplified VFF potential, and the results indicate that, when the full system is excited with the initial condition given by the fixed point in the Poincaré section of the RS, the long-lived DB solution can be observed, which emerges only when the energy is larger than a threshold value. A short summary and discussion is presented in Sec. V.

II. THE NONLINEAR HONEYCOMB LATTICE

The dynamical system in this work is a nonlinear honeycomb lattice which can be regarded as a simplified abstract model of graphene sheet. Figure 1 shows the schematic of the nonlinear honeycomb lattice, and in our simulations, we have used a system with 4800 sites to reduce the finite size effects. The interactions between adjacent sites is a simplified version of the VFF potential [52,53], which was proposed by Lobo *et al.* in 1997 for systems whose interactions between carbon atoms are the sp^2 bonds, such as graphene and fullerenes. The expression of the VFF potential is given by [52,53]

$$U_{sp^2} = \sum_{i=1}^{N} \gamma \boldsymbol{D}_i \cdot \boldsymbol{D}_i + \frac{1}{2} \sum_{i=1}^{N} \sum_{j} \frac{\alpha}{4a_0^2} \left(\boldsymbol{r}_{ij}^2 - a_0^2\right)^2 + \sum_{i=1}^{N} \sum_{j<k} \frac{\beta}{a_0^2} \left(\boldsymbol{r}_{ij} \cdot \boldsymbol{r}_{ik} + \frac{1}{2} a_0^2\right)^2, \quad (1)$$

where $\alpha = 155.9$ J/m^2, $\beta = 25.5$ J/m^2 and $\gamma = 7.4$ J/m^2 are constants, index i labels the sites, indices j and k label the nearest neighbors of site i, N is the system size or the number of atoms, $\boldsymbol{r}_{ij}$ is the bond vector from site i to j, $a_0 = 1.421$ Å is the equilibrium bond length, and $\boldsymbol{D}_i = \sum_j \boldsymbol{r}_{ij}$ is the dangling bond vector introduced by Chelikowsky *et.al.* in predicting the three dimensional structure of silicon clusters, which can characterize the transfer of dangling bond strength to backbonds [54]. The first term accounts for the variation of angle between the neighboring p_z-orbitals approximately perpendicular to the graphene plane, which gives the quadratic energy in displacement for the out-of-plane deformation [54–56]. The second and third terms characterize the change of bond length and angle between the adjacent C-C bonds, respectively.

Nanoelectromechanical resonators based on 2D materials have become an important topic due to its ultra-high mechanical vibration frequency and ultra-low energy consumption and thus potential engineering applications [57–59]. For graphene resonators, the graphene sheets are deposited on the substrate with a trench, and the suspended part can be actuated electrically or optically and will vibrate along the direction perpendicular to the graphene plane [60–62]. The preliminary numerical simulations exhibit that the magnitude of the in-plane motion is few orders smaller than that of the out-of-plane motion under the initial condition where the graphene sheet is deformed according to the fundamental mode. As a result, we only consider the out-of-plane motion, i.e., the motion along z-direction, and Eq. (1) can be simplified as

(Appendix A):

$$U_{sp^2} = \sum_{i=1}^{N} \gamma \left(\sum_j z_j - 3z_i \right)^2 + \frac{1}{2} \sum_{i=1}^{N} \sum_j \frac{\alpha}{4a_0^2} (z_j - z_i)^4 + \sum_{i=1}^{N} \sum_{j<k} \frac{\beta}{a_0^2} [(z_j - z_i)(z_k - z_i)]^2 = U^{(2)} + U_1^{(4)} + U_2^{(4)}. \quad (2)$$

Here z_i is the displacement of site i from its equilibrium position. It is clear that the orders of $U^{(2)}$, $U_1^{(4)}$, and $U_2^{(4)}$ are 2, 4, and 4, respectively, which is very similar with the potential of the FPUT-β lattice where each site interacts only with its nearest neighbors. For the VFF potential, the net force acting on site i comes from its nearest and next-nearest neighbors. This simplified VFF model has been employed in our previous works investigating energy equipartition problem in graphene resonators with fixed boundary conditions [51,63], and it has been demonstrated that the nonlinear honeycomb lattice with potential Eq. (2) is an excellent platform for examining various dynamical behaviors.

As mentioned above, the phonon band edge plays an important role in the formation of the DBs. For the unstrained graphene where all the carbon atoms locate at the equilibrium position, the lower band edge approaches to zero, and there is no gap between the branches. Thus, to stay outside the phonon bands and to prevent phonon scattering, the DBs can only exist above the upper phonon band edge. The dispersion relation of Eq. (2) is presented in Appendix B, and the maximum of the ZO branch is only determined by the parameter γ in $U^{(2)}$ with the following expression [52]:

$$f_u = \frac{1}{2\pi} \sqrt{72\gamma / m_C} = 26.025 \text{ THz}, \quad (3)$$

where $m_C = 1.9926 \times 10^{-26}$ kg is the mass of the carbon atom. In addition, the bond between adjacent atoms is effectively a hard-type spring, that the frequency will increase when the amplitude of vibration becomes larger [64]. This is actually a necessary condition for this system to sustain DBs, that when its amplitude is large enough the frequency can go beyond the upper band edge.

To reduce the numerical error, the parameters $m_0 = 1.9926 \times 10^{-26}$ kg, $a_0 = 1.421 \times 10^{-10}$ m, and $t_0 = 1.0 \times 10^{-14}$ s are used to nondimensionalize the equation of motion. Then the mass of the sites and the equilibrium bond length become unit, the dimensionless constants α', β' and γ' are 0.7824, 0.1280, and 0.0371, respectively, and the dimensionless upper phonon band edge f_u' is 0.2603.

The MD simulations are performed with potential Eq. (2), which means that the in-plane motion of each atom is constrained. The Verlet algorithm with a time step 0.001 is used for the integration of the Newtonian equations of motion of the sites. The periodic boundary conditions are applied on both x and y directions, which is the conventional setup in the investigation of DBs. We have performed the MD simulations with both fixed and periodic boundary conditions, and the results are very similar when the system size is large enough. That is to say, the DBs also exist in the system with fixed boundary condition, which is just the circumstance for the graphene resonators.

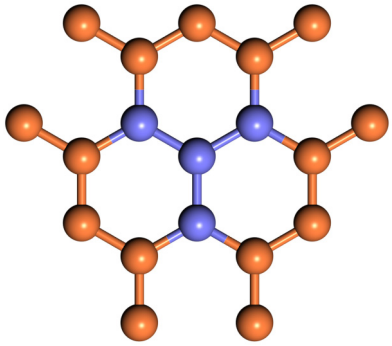

FIG. 2. The reduced system. Blue sites are able to move in the force field, while the red ones are fixed during the numerical simulation. According to the expression of Eq. (2), all the nearest and second nearest neighbors of movable sites should be appended to the system.

III. DYNAMICS OF THE REDUCED SYSTEM

A. The reduced system

Due to the peculiar properties of DBs, they are highly localized in real space, i.e., only a few sites near the central one oscillate with relatively large amplitude, while most of the other sites are nearly frozen around the equilibrium position. In addition, as the frequency of the DB is usually higher than the phonon band edge, the coupling between the DBs and the phonons is negligible, thus the energy transfer from the DB to phonons is almost prohibited. In this sense, we can only consider the dynamics of the sites near the central site belonging to the breathers. This scheme is called reduced problem, which was first proposed by Flach *et al.* [28,40,41] and has been applied to search the DBs in one-dimensional nonlinear discrete Klein-Gordon lattice [40] and 2D discrete Hamiltonian lattice [28].

It is expected that the size of the DBs in 2D nonlinear honeycomb lattice is small. As a reasonable guess, we assume that the DBs contain only four sites: a central site and its three nearest neighbors, as illustrated by the blue sites in Fig. 2. Except the movable sites, the RS also contains fifteen fixed sites, e.g., all the nearest and second-nearest neighbors of the movable sites, to ensure that the potential of the movable sites can be calculated self-consistently. Obviously, the RS is a model with threefold rotational symmetry. There will be motions that all the nearest neighbors of the central site move synchronously. In this regard, the dynamics of the RS can be reduced to a two degrees-of-freedom, and its Hamiltonian can be written as

$$H = \tfrac{1}{2} v_0^2 + \tfrac{3}{2} v_1^2 + U_{sp^2}(z_0, z_1), \quad (4)$$

where v_0 (v_1) and z_0 (z_1) are the velocity and displacement of the central site (its nearest neighbors), respectively. The first two terms are the kinetic energies of the corresponding sites, and the third term is the potential energy given by Eq. (2), which is zero when all the sites are at rest in the equilibrium position.

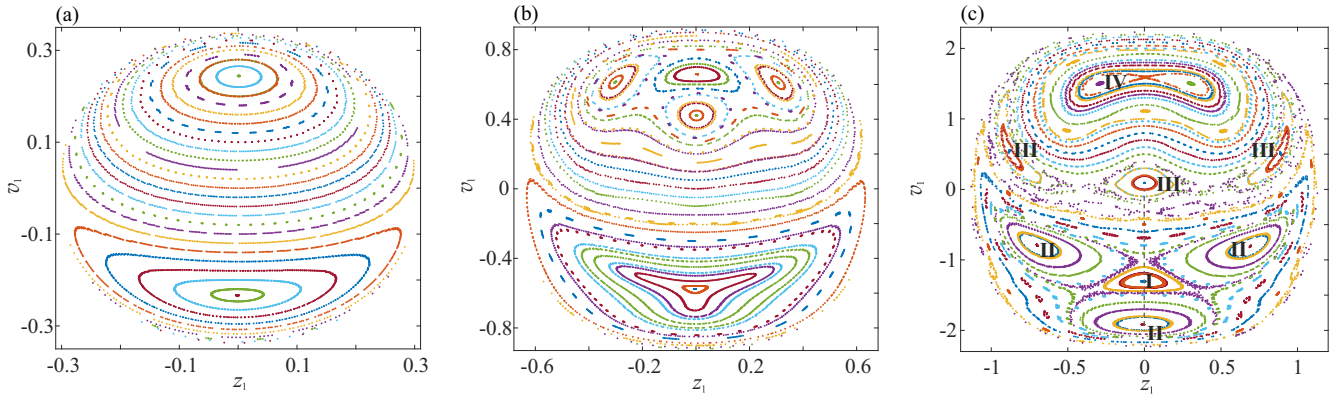

FIG. 3. (a)–(c) Poincaré sections between the trajectories and the subspace $[z_1, v_1, z_0 = 0, v_0 > 0]$. The initial excitation energies E for (a)–(c) are 0.17, 1.30, 7.50, respectively. The trajectories with different colors in the same panel correspond to different initial conditions with the same excitation energy. In panel (c), the fixed points (periodic orbits) are labeled by I–IV, which are the promising candidates for DBs of the full system. The vertical gray dashed line in panel (c) gives the initial conditions used in Fig. 6.

B. Dynamics of the RS

The dynamical behaviors of the RS can be illustrated with the Poincaré section between the trajectory and the subspace $[z_1, v_1, z_0 = 0, v_0 > 0]$. For this purpose, the RS is actuated with a series of initial conditions which have the same excitation energy E: The displacements of all the sites are set to zero, and the initial velocity $v_0 > 0$ and v_1 are assigned to the central site and its three nearest neighbors, and $E = \frac{1}{2}v_0^2 + \frac{3}{2}v_1^2$. Then the MD simulations are performed in the RS with these initial conditions, and the positions and velocities of all the sites are collected every few steps to draw the Poincaré section. Note that some orbits may be missed with such setup, resulting in some blank areas in the Poincaré section. In this case, additional initial conditions chosen from these areas can be used to fill up the whole space of the intersection.

Figure 3 shows the Poincaré sections of the RS with three representative excitation energies. (i) For small energy, Fig. 3(a) exhibits that the motions of the sites are regular with two fixed points in the upper and lower part of the Poincaré section, which correspond to periodic trajectories in phase-space. Around them are a series of quasiperiodic orbits. (ii) As the initial excitation energy E becomes larger, a period-3 orbit arises near the original upper fixed point, as shown in Fig. 3(b). Another interesting change is that the quasiperiodic trajectories near the fixed point in the lower part of the intersection are evidently deformed, i.e., three sharp corners gradually emerge. (iii) As the excitation energy increases further, the dynamics of RS become more complicated. Figure 3(c) shows the Poincaré sections for $E = 7.50$. The period-3 orbit of the upper plane moves outward further, as marked by III, and the central fixed point becomes unstable, generating two stable fixed points (periodic orbits) at the left and right side (IV). Note that the two fixed points represent two antisymmetric $[z_0(t) \to z_0'(t), z_1(t) \to z_1'(t)]$ but disconnected periodic orbits. On the lower plane, the deformed corners around the central fixed point (I) are detached and form a new period-3 orbit II. This transition occurs around $E = 1.30$. In the meantime, chaotic sea emerges. We have calculated more cases with larger excitation energies, and the structure of the Poincaré section will not change qualitatively except that the area of chaotic sea becomes larger.

We shall focus on the periodic orbits (fixed points in the Poincaré section) as they are the potential candidates for the exact solutions of DBs. Figures 4(a)–4(d) show the time evolutions of the sites for the same time window with respect to the orbits I–IV in Fig. 3(c), respectively. The central site and its nearest neighbors vibrate inversely for orbits I [Fig. 4(a)] and in phase for orbit IV [Fig. 4(d)]. The data given by the black asterisks are those drawn on the Poincaré sections. For orbits II and III, the vibrations of the central site and its nearest neighbors are a little more complicated as they are both period-3 orbits [Figs. 4(b) and 4(c)]. In the next section, orbits I–IV are set as the initial conditions to search for the DB solutions in the full system.

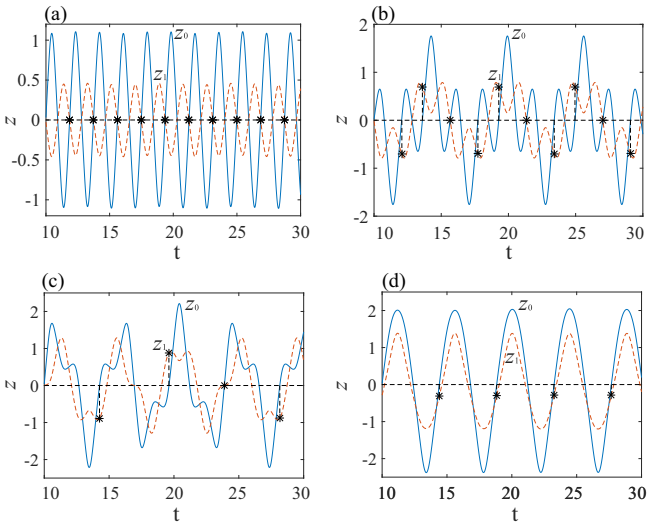

FIG. 4. (a)–(d) The time evolution of the displacements of the central site (blue solid line) and its nearest neighbor (red dashed line). Panels (a)–(d) correspond to the initial conditions labeled by I–IV in Fig. 3(c), respectively. The black asterisks are the points drawn in the Poincaré sections.

IV. DBs IN THE FULL SYSTEM

A. Existence of DBs

From now on, we search the DB solutions for the nonlinear honeycomb lattice with MD simulations in the full system which contains 4800 sites in total. One of the sites of the graphene sheet is chosen as the central site, and at $t = 0$ s, all the sites are placed at their equilibrium positions except the central particle and its nearest neighbors, which are displaced according to the periodic orbit found in the RS. Then the full system evolves at the microcanonical ensemble for 1.0×10^7 steps, and the displacements and velocities of all the sites are recorded every few steps for further investigation. When DBs exist, the energy of the system will be localized in the space near the central site, where the other sites of the system remain almost static. In this sense, the DBs can be characterized by the ratio of the local energy E_L to the total energy E_T of the full system, i.e.,

$$\eta = \frac{E_L}{E_T}, \tag{5}$$

where E_L is defined as the summation of the energy of the central site, its nearest and second-nearest neighbors [the 10 red sites in the insets of Figs. 5(b) and 5(c)], and E_T is the total energy of all the sites, which is naturally equal to the excitation energy initially fed into the system.

Figure 5(a) shows, for a given initial excitation energy $E_T = 7.5$ [the same for Fig. 3(c)], the time evolution of η, where the initial conditions are given by the orbits I–IV in Fig. 3(c). For orbit I, it is a fixed point in the RS. It can be seen that, when the full system is actuated with this initial condition, only a tiny fraction of the initial excitation energy dissipates to the other part of the system, i.e., $\eta \simeq 1$, and then the local energy E_L stabilizes with a small fluctuation for a long time. Figure 5(b) is the Fourier spectrum of the trajectories of the central site. The dynamical behaviors of the local vibration can be characterized by the two main frequencies, marked by f_1 and f_2 in Fig. 5(b), and the other peaks can be given by the linear combinations of these two frequencies. It can be inferred that this is a quasiperiodic DB solution for the nonlinear honeycomb lattice. The verification of the existence of DBs can also be read out from the energy distribution versus the particle position, where the central site has the largest energy while the sites out of the RS have negligible values [inset of Fig. 5(b)].

For the RS, orbit II exists only when the energy is larger than 1.33. When it is set as the initial condition for the MD simulation of the whole system, more energy than that for orbit I is transferred out from the local region of the RS around $t = 10 \sim 20$ of the MD simulations [Fig. 5(a)]. But after a short transition, the ratio of the energy is almost stabilized around $\eta \sim 0.85$ for a long time, indicating the possibility of a DB solution. We have then plotted the Fourier spectrum for orbit II in the stable region for t from 5000 to 10 000, which shows very similar results as that for orbit I, as shown in Fig. 5(c). Therefore, it can be conjectured that: For orbit II, after a part of the excitation energy escapes from the local excited region, the remaining energy redistributes among the localized sites and the dynamics are attracted to the DB initialized from orbit I. But since the outer sites are excited too, the DB is less stable that it has a shorter life time.

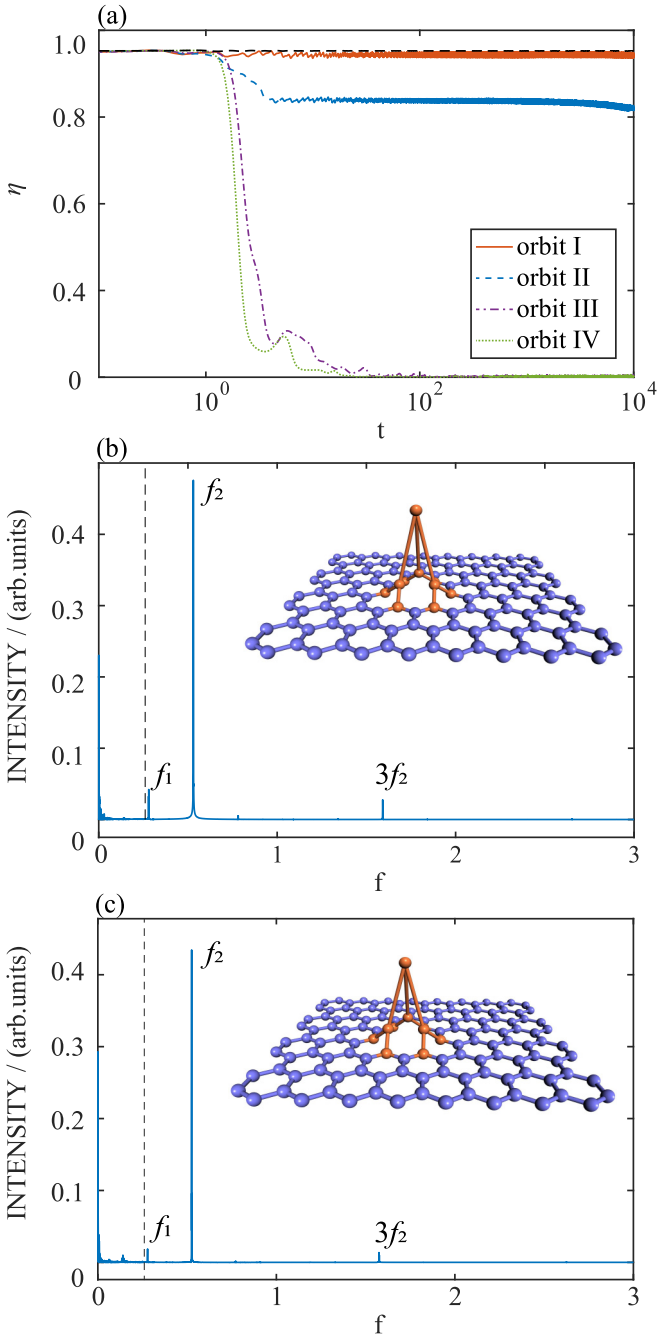

FIG. 5. (a) The time evolution of the ratio η where the initial conditions in the MD simulations are chosen from the orbits I-IV of the RS in Fig. 3(c). The black dashed line indicates $\eta = 1$. (b), (c) The Fourier spectrum of $z_0(t)$ for the orbits I and II presented in panel (a), respectively. $f_1 = 0.280$, $f_2 = 0.533$ for panel (b) and $f_1 = 0.276$, $f_2 = 0.511$ for panel (c). Note that the nondimensionalized upper band edge is $f_u' = 0.2603$, as marked by the vertical dashed line. The insets show the energy distribution for the sites near the central one, where the height of each site represents its total energy.

To verify this conjecture, a set of MD simulations are performed with the same excitation energy $E = 7.50$, but the initial conditions are uniformly picked up from the

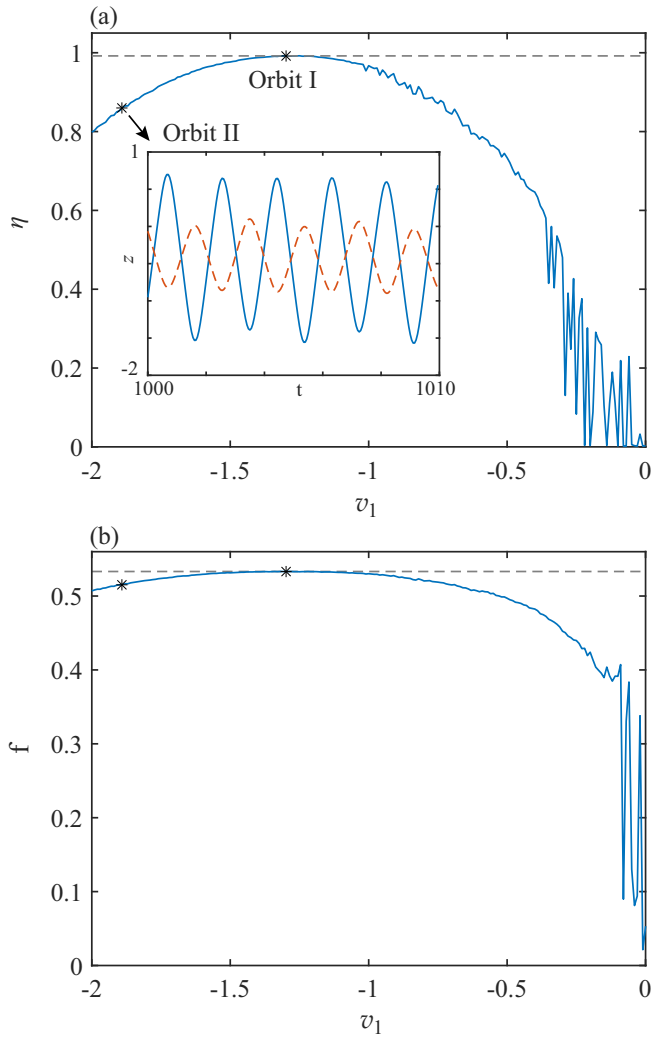

FIG. 6. (a) Dependence of the average of η [Eq. (5)] from $t = 5000$ to $t = 10\,000$ on the initial velocity v_1 for the same excitation energy $E = 7.50$, where the initial conditions for MD simulations are uniformly picked from the segment $\{(z_1, v_1)|z_1 = 0, -2 < v_1 < 0\}$ in Fig. 3(c). The inset shows the trajectories of the central particle $z_0(t)$ and its nearest neighbors $z_1(t)$ when the initial condition is on orbit II. (b) The frequency for the dominant peak in the Fourier spectrum of $z_0(t)$ under the same initial conditions in panel (a). In both panels, the orbits I ($v_1 = -1.30$) and II ($v_1 = -1.89$) are marked by black asterisks.

segment $\{(z_1, v_1)|z_1 = 0, -2 < v_1 < 0\}$ in the Poincaré section in Fig. 3(c), as indicated by the gray dashed line, which covers the orbit I and II of the RS. Figure 6(a) shows the dependence of η on the velocity v_1, where the orbit I and II are marked by black asterisks.

It can be seen that η has the largest value for orbit I, and then decreases gradually as the initial condition v_1 deviates this point from both sides. Note that since the localized energy E_L only counts about 10 sites around the central site, and the system has in total 4800 sites, thus if there is no DB, the value of η will be round 0.002. Thus, all the apparent nonzero values of η indicate the formation of DBs, e.g., $-2 < v_1 < -0.4$ in this figure. An apparent evidence is presented in the inset of Fig. 6(a), which plots the trajectories of $z_0(t)$ and $z_1(t)$ when the full system is excited with orbit II, and shows very similar behavior with the one for orbit I in Fig. 4(a). This provides direct evidence of the above conjecture. Furthermore, we have checked the trajectories of $z_0(t)$ and $z_1(t)$ for various different parameter values in the range $-2 < v_1 < -0.4$, and they all have the similar dynamics as that for orbit I (Appendix C). This strongly supports the physical picture that for initial values around orbit I, after shedding some energy into other parts, the remaining energy reforms a DB in the form close to orbit I.

In addition, the ratio η tends to zero with large fluctuations as the initial velocity v_1 approaches to zero. Since $E_T = \frac{1}{2}v_0(0)^2 + \frac{3}{2}v_1(0)^2$, $v_1(0)$ approaches zero is the case that the energy is injected almost only to the central site. In this case, the energy will be soon dissipated to the whole system and no DB will be formed. This illustrates the importance of the nearest-neighboring sites of the central site, that although their energy is small compared to the central site, maintaining a proper vibration of these sites is necessary for the formation of the DB. Figure 6(b) shows the corresponding frequency of the highest peak of Fourier spectrum of $z_0(t)$ for the simulations in Fig. 6(a). The local vibration of the central site spontaneously has the largest frequency for initial excitations on orbit I. The reason is that the frequency is positively dependent on the energy of vibration in nonlinear system, and since the remaining energy reaches maximum at orbit I, the frequency also peaks at the same value [Fig. 6(b)].

The dynamics of the whole system with initial excitations on orbits III and IV are quite different from that for orbits I and II. The energy fed into the system at the beginning spreads rapidly to the other parts of the system, resulting in delocalization of the energy. A series of the profile snapshots of the system when the full system is actuated with orbit IV are shown in Appendix D. It can be seen that the energy will flow to the other parts in a wave form, e.g., like the waves spreading outwards from the center when a stone is dropped into the water. We have also calculated more cases with higher excitation energies, and DBs are never observed, even when the frequencies of the orbits are higher than the phonon band edge. This implies that not every periodic orbit of the RS gives rise to a DB of the full system, e.g., in our case, only orbit I successes to excite a DB.

B. Energy threshold

After the verification of the DB solutions, the next natural step is to find out the parameter range where the DBs can exist for a long time. Based on previous theories, when the frequency of the orbit is smaller than the upper phonon band edge, the localized vibration can be scattered by the phonons, which results in the annihilation of the DB solutions. Thus, there might be an energy threshold for the long-lived DBs. Here we perform MD simulations with the initial conditions on orbit I versus the variation of the energy, and the ratio η is estimated. Note that, the fixed point orbit I depends on the initial excitation energy, which can be determined from the dynamics of the RS.

Figure 7(a) shows the dependence of η on the initial excitation energy when orbit I is used to excite the full system. For small energy ($E < 0.49$), the frequency of the local

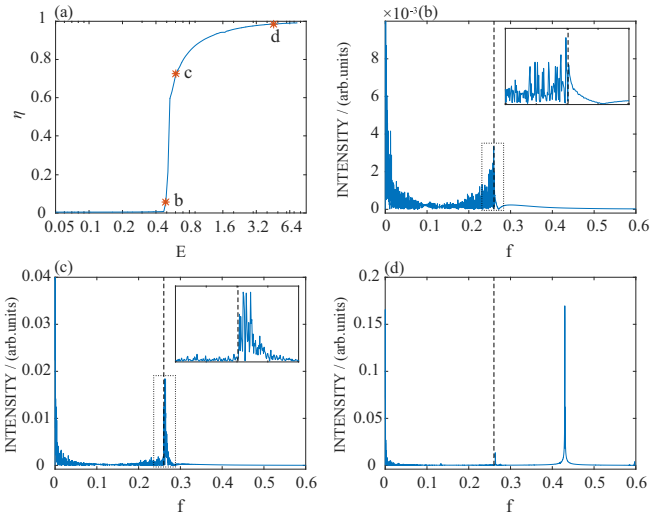

FIG. 7. (a) Ratio η versus initial excitation energy when the full system is excited according to orbit I of the RS. Note that the x axis is in the logarithmic scale. (b)–(d) The Fourier spectrum for the trajectory of the central site. The excitation energies are 0.49, 0.61, and 4.60, which are marked by red asterisks and correspondingly denoted by b, c, d in panel (a). The vertical dashed line indicates the upper phonon band edge f_u'. The insets in panels (b, c) zoom in the region indicated by the black dotted rectangles to demonstrate clearly the spectral properties around f_u'.

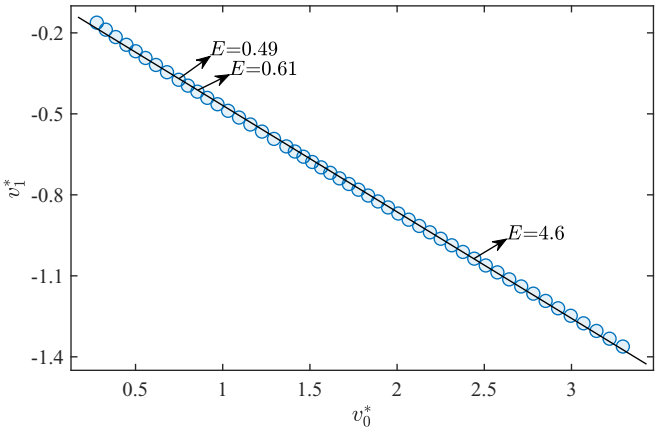

FIG. 8. The fixed point (v_0^*, v_1^*) for different energies in the subspace $[z_1, v_1, z_0 = 0, v_0 > 0]$ used in Fig. 7(a). The blue circles are directly read from the Poincaré section, and the black solid line is fitted with $v_1^* = kv_0^* + b$, where k and b are -0.3944 and -0.0744, respectively. The initial condition for Figs. 7(b)–7(d) are marked by black arrows.

excitation is smaller than the phonon band edge, and the energy flow pathway can be established via the interaction between phonons and the local vibrations. Under such condition, nearly all the excitation energy transfers to the other part of the system, and the initially excited sites are indistinguishable from the other sites based on their dynamical behaviors. As the excitation energy increases, the frequency of the vibration becomes larger, and will pass the linear phonon band edge at some point. It can be seen that a sharp rise of η is observed for $E > 0.49$, which indicates that a large proportion of the energy is localized in a small area near the central site, indicating the formation of the DB. But since the energy will be dissipated, the dynamics of the DB is different from that of the orbit I in the RS. As the energy increases further, η gradually approaches to 1, where most of the energy is localized, and the dynamics of the orbit I approximates the DB of the full system well. In this sense, the reasonable choice of energy threshold for the formation of DBs is $E_c = 0.49$, which corresponds to 12.32 eV.

This energy threshold originates from the fact that the frequency of the local vibration just passes the upper band edge at E_c. To elucidate this point, Figs. 7(b)-7(d) show the Fourier spectrum with three representative excitation energies marked by red asterisks in Fig. 7(a). For case b, most of the Fourier spectrum peaks are below the upper phonon band edge. But as the inset of Fig. 7(b) shows, there is a peak, although small, above the phonon band edge, indicating that the DB starts to form at this energy. Figure 7(b) also exhibits the energy flow pathway from the local excitation to the phonons, i.e., the thermalization process. Due to the resonance between phonons and the DBs, the energy initially injected into the system spreads to the phonons whose frequencies are close to the upper band edge, and also to the ones which have the same wave vectors in the acoustic branch. These phonons are close to the Γ point in the first Brillouin zone. The intermodal energy transfer between the phonons with the same wave vectors in different branches has been investigated in detail in Refs. [51,63]. For case c, the dominant frequency of the local vibration is obviously larger than the band edge. Although the component for small frequency ($f \sim 0$) is still large, those close to but below the band edge are significantly suppressed [Fig. 7(c)]. Comparing to Fig. 7(b), it seems that the energy for these frequency components are absorbed by the DB whose dominant frequency is a little bit higher than the band edge. As the energy increases further, most of the energy becomes localized around the central site, and there are only a few sharp peaks in the Fourier spectrum, while all the other frequency components are suppressed. This implies the existence of the long-lived DBs in the full system [Fig. 7(d)]. These results clearly reveal the dynamical behaviors of the formation of the DBs.

It can be concluded that the DB solutions of the nonlinear honeycomb lattice can be excited with orbit I of the RS. A natural question is that whether we can find a simple expression for the dependence of orbit I on the excitation energy. For now, for each initial excitation energy, we need to plot the Poincaré section to determine the parameters for orbit I. If a simple expression is available, then the initial condition for generating DBs can be obtained much easier. According to the Poincaré section, one has $z_1 = 0$ for orbit I in the subspace $[z_1, v_1, z_0 = 0, v_0 > 0]$, which means that this orbit can be determined uniquely from the velocities v_0 and v_1 of the sites. Figure 8 presents (v_0^*, v_1^*) for the fixed points for orbit I, for different initial excitation energies, where v_1^* is directly picked up from the Poincaré section, and v_0^* is obtained from the relation $E = \frac{1}{2}v_0^{*2} + \frac{3}{2}v_1^{*2}$ with the condition that the sign of v_0^* is different from that of v_1^*. The data can be fitted with a linear function $v_1^* = kv_0^* + b$ very well, where k and b are -0.3944 and -0.0744, respectively. Substituting back to the

expression for energy E, one can obtain v_0^* directly by solving the following equation:

$$E = \tfrac{1}{2}v_0^{*2} + \tfrac{3}{2}(kv_0^* + b)^2. \tag{6}$$

Then together with $v_1^* = kv_0^* + b$, one can yield the pair of (v_0^*, v_1^*) as the initial conditions for DBs as $z_0 = 0$ and $z_1 = 0$ are already known as a precondition, when E is above the threshold. In addition, the data points for E below the threshold are also plotted. They follow the same relation $v_1^* = kv_0^* + b$ reasonably well. This shows the continuity of the dependence of orbit I on the energy, but only when the energy is above the threshold, it is relevant to guide to the DBs.

Note that in our simulations, we only consider the out-of-plane motions. The maximum of the LO and TO branches of the phonon band of the full VFF model is 47.6 THz [52], which is much higher than that of the ZO branch, i.e., 26.02 THz. In this sense, the DBs in this work in general can be scattered by the in-plane modes, which will lead to the reduction of the lifetime of the DBs. We have performed preliminary simulations when the full system is actuated with orbit I of the RS, where both the full [Eq. (1)] and simplified [Eq. (2)] VFF models are employed in the simulations. It is found that the energy ratio η with the full model is always smaller than that with the simplified one because of the scattering induced by the in-plane phonons. When the excitation energy is relatively small but larger than the threshold $E_c = 0.49$, e.g. $E = 1.0$, the simulations with the full model exhibit that more than 70% of the excitation energy can be localized in the small region surrounding the initially excited sites for a long time (at least 10^4), which corroborates the survival of the DBs in the full VFF model. This ascribes to the weak coupling between in-plane and out-of-plane modes. However, the energy ratio η becomes smaller as the excitation energy increases due to the stronger scattering by the in-plane modes. As an example, when the excitation energy is 2.5, the ratio η decreases to zero at $t \simeq 5000$, which indicates the thorough annihilation of the DBs.

V. SUMMARY AND DISCUSSION

In summary, the DBs and their induced energy localization have been systematically investigated in the nonlinear honeycomb lattice with the dynamics of the two degree-of-freedom RS and extensive MD simulations in the full system. For the RS, the periodic orbits are obtained by calculating the fixed points in the Poincaré sections, and four different types of periodic orbits are identified. These orbits are possible candidates for DBs. This indeed is true for orbit I, where the MD simulations in the full system with initial conditions given by this orbit I supply clear evidence for the emergence of a stable DB solution for the nonlinear honeycomb lattice. Furthermore, when the other orbits (including orbit II) near this fixed point are employed as the initial condition, the dynamics of the local vibrations will also be attracted to a DB similar to orbit I after a transient process where part of the excitation energy spreads out to the other part of the system. For initial conditions on orbits III and IV, the initial excitation energy flows to the other part of the full system quickly in a wave propagating form, resulting in delocalization of the vibration. Systematic MD simulations indicate that there is an energy threshold that above which the DB can survive in the full system for a long time. When the excitation energy is not large enough, the energy will be dissipated, and the energy flow pathway between the local excitation and the phonons has also been identified.

We have provided a complete physical picture for the dynamical behaviors of the nonlinear honeycomb lattice under specific local excitations, which will be crucial to the understanding of the local integrability of nonlinear lattices, and to the analysis of mechanical vibrations of graphene based nanodevices. Thanks to the advances in nanotechnology, the atomic scale phenomena can be directly investigated in the cutting-edge experiments [57]. For larger nano- and microelectromechanical systems made from graphene, continuum description generally works well [61]. Nevertheless, due to the impact on the properties of the entire system, the atomic scale phenomenon can also be identified in larger systems. For instance, since the DBs are mainly scattered by the phonons near the Γ point in the first Brillouin zone, the measurement of the populations [65] can be exploited to infer the existence of the DBs. The DBs can result in the Stone-Wales defects [66], which can be observed by scanning transmission electron microscopy [67]. In addition, our results also demonstrate the power of the reduced problem method for searching DBs, which are expected to find broader applications in nonlinear lattices abstracted from other 2D materials.

ACKNOWLEDGMENTS

We thank Prof. Yong Zhang for illuminating discussions. This work was supported by NSFC under Grants No. 11905087, No. 11775101, No. 12175090, and No. 12047501, and by the Natural Science Foundation of Gansu Province under Grant No. 20JR5RA233.

APPENDIX A: DEDUCTION FROM Eq. (1) TO Eq. (2)

The empirical potential is

$$U_{sp^2} = \sum_{i=1}^{N} \gamma \boldsymbol{D}_i \cdot \boldsymbol{D}_i + \frac{1}{2}\sum_{i=1}^{N}\sum_{j} \frac{\alpha}{4a_0^2}\left(\boldsymbol{r}_{ij}^2 - a_0^2\right)^2 + \sum_{i=1}^{N}\sum_{j<k} \frac{\beta}{a_0^2}\left(\boldsymbol{r}_{ij}\cdot\boldsymbol{r}_{ik} + \frac{1}{2}a_0^2\right)^2. \tag{A1}$$

The bond vector between atom i and its nearest neighbor j can be written as

$$\mathbf{r}_{ij} = (x_j - x_i)\mathbf{e}_x + (y_j - y_i)\mathbf{e}_y + (z_j - z_i)\mathbf{e}_z, \tag{A2}$$

where $\mathbf{e}_x$, $\mathbf{e}_y$, and $\mathbf{e}_z$ are the units vectors in Cartesian coordinates. By fixing the motions along x and y direction, (a) it is easily inferred that

$$\mathbf{r}_{ij}^2 = a_0^2 + (z_j - z_i)^2, \tag{A3}$$

as $a_0^2 = (x_j - x_i)^2 + (y_j - y_i)^2$ gives the equilibrium bond length; (b) the dangling bond vector is

$$\begin{aligned} \boldsymbol{D}_i &= \sum_j \mathbf{r}_{ij} \\ &= \left(\sum_j x_j - 3x_i\right)\mathbf{e}_x + \left(\sum_j y_j - 3y_i\right)\mathbf{e}_y \\ &\quad + \left(\sum_j z_j - 3z_i\right)\mathbf{e}_z \\ &= \left(\sum_j z_j - 3z_i\right)\mathbf{e}_z, \end{aligned} \tag{A4}$$

where the terms $\sum_j x_j - 3x_i$ and $\sum_j y_j - 3y_i$ are always zero due to the special structure of honeycomb lattice; (c) the dot product $\boldsymbol{r}_{ij} \cdot \boldsymbol{r}_{ik}$ is

$$\begin{aligned} \boldsymbol{r}_{ij} \cdot \boldsymbol{r}_{ik} &= (x_j - x_i)(x_k - x_i) + (y_j - y_i)(y_k - y_i) \\ &\quad + (z_j - z_i)(z_k - z_i) \\ &= -\tfrac{1}{2}a_0^2 + (z_j - z_i)(z_k - z_i), \end{aligned} \tag{A5}$$

where $(x_j - x_i)(x_k - x_i) + (y_j - y_i)(y_k - y_i) \equiv -1/2a_0^2$ as all the angles are $2/3\pi$ for the graphene at their equilibrium positions. Substituting Eqs. (A2)–(A5) into Eq. (A1), we have

$$\begin{aligned} U_{sp^2} &= \sum_{i=1}^{N} \gamma \left(\sum_j z_j - 3z_i\right)^2 + \frac{1}{2}\sum_{i=1}^{N}\sum_j \frac{\alpha}{4a_0^2}(z_j - z_i)^4 \\ &\quad + \sum_{i=1}^{N}\sum_{j<k} \frac{\beta}{a_0^2}[(z_j - z_i)(z_k - z_i)]^2. \end{aligned} \tag{A6}$$

APPENDIX B: DERIVATION OF DISPERSION RELATION

The dispersion relation of Eq. (2) can be obtained with the lattice dynamics method. The basic idea is to solve the following equation:

$$\omega^2(\mathbf{k}, \nu)\mathbf{e}(\mathbf{k}, \nu) = \mathbf{D}(\mathbf{k}) \cdot \mathbf{e}(\mathbf{k}, \nu), \tag{B1}$$

where $\mathbf{D} = [D_{ij}]_{2\times 2}$ is the stiffness matrix:

$$D = \begin{bmatrix} D_{11} & D_{12} \\ D_{21} & D_{22} \end{bmatrix}. \tag{B2}$$

The element D_{ij} of the matrix is given by

$$\begin{aligned} D_{11} &= \frac{2\gamma}{m}(12 + \mathrm{e}^{i\mathbf{k}\cdot(\mathbf{a}_1 - \mathbf{a}_2)} + \mathrm{e}^{-i\mathbf{k}\cdot\mathbf{a}_2} + \mathrm{e}^{-i\mathbf{k}\cdot\mathbf{a}_1} \\ &\quad + \mathrm{e}^{-i\mathbf{k}\cdot(\mathbf{a}_1 - \mathbf{a}_2)} + \mathrm{e}^{i\mathbf{k}\cdot\mathbf{a}_1} + \mathrm{e}^{i\mathbf{k}\cdot\mathbf{a}_2}), \\ D_{12} &= -\frac{12\gamma}{m}(1 + \mathrm{e}^{-i\mathbf{k}\cdot\mathbf{a}_2} + \mathrm{e}^{-i\mathbf{k}\cdot\mathbf{a}_1}), \\ D_{21} &= -\frac{12\gamma}{m}(1 + \mathrm{e}^{i\mathbf{k}\cdot\mathbf{a}_2} + \mathrm{e}^{i\mathbf{k}\cdot\mathbf{a}_1}), \\ D_{22} &= D_{11}, \end{aligned} \tag{B3}$$

where $\mathbf{k} = k_x\mathbf{e}_x + k_y\mathbf{e}_y$ is the wave vectors, $\mathbf{a}_1$ and $\mathbf{a}_2$ are the unit-cell vectors as shown in Fig. 9(a). Substituting Eqs. (B2) and (B3) into Eq. (B1), the frequency is

$$\omega^2 = \frac{2\gamma}{m}(12 + g(\mathbf{k})) \pm \frac{12\gamma}{m}\sqrt{3 + g(\mathbf{k})}, \tag{B4}$$

where

$$g(\mathbf{k}) = 2\cos(\sqrt{3}k_y a) + 4\cos\left(\frac{3k_x a}{2}\right)\cos\left(\frac{\sqrt{3}k_y a}{2}\right). \tag{B5}$$

Figure 9(b) shows the dispersion relation given by Eq. (B4). For the optical phonon in the Brillouin zone center, the wave vector $\mathbf{k}$ is zero, i.e., $k_x = k_y = 0$, and Eq. (B5) and Eq. (B4) become $g(\mathbf{k}) = 6$ and $\omega_{\max} = \sqrt{72\gamma/m_C}$, respectively. The later one is just the Eq. (3) in the paper.

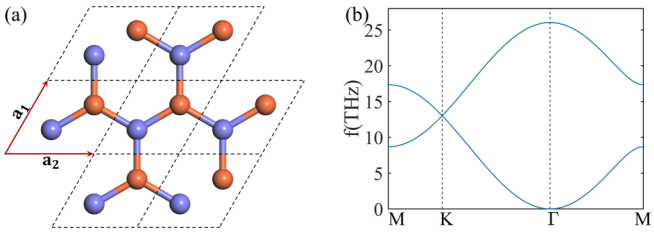

FIG. 9. (a) Schematic of graphene lattice. (b) Dispersion relation of graphene derived from Eq. (2) with lattice dynamics method.

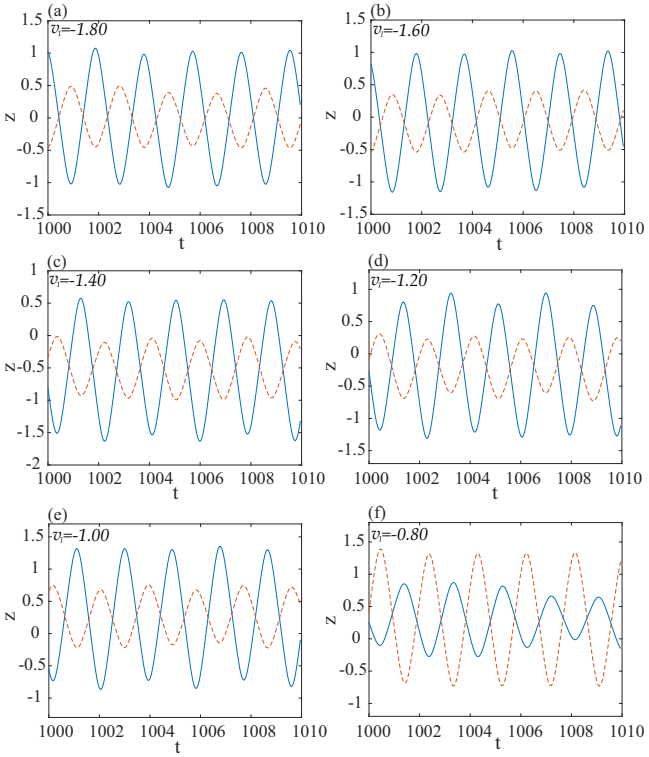

FIG. 10. (a)–(f) Time evolutions of the displacements of the central site (blue solid line) and its nearest neighbors (red dashed line). The initial conditions of $v_1(0)$ are chosen from Fig. 6, i.e., the system is actuated with the same excitation energy $E = 7.50$, and $z_1(0) = 0$. Note that $v_1(0) = -1.30$ for orbit I.

APPENDIX C: REPRESENTATIVE TRAJECTORIES IN FIG. 6

Here we supply more evidence for the conjecture that the trajectories whose initial condition is close to orbit I are attracted to orbit I of the RS. Figure 10 exhibits six representative trajectories of the central site and its nearest neighbors, where the initial velocities v_1 are shown in the upper left corner of each panel. It can be seen that all the trajectories are similar to that for the orbit I shown in Fig. 4(a), and the amplitude of the oscillation is larger as $v_1(0)$ is close to that for orbit I.

APPENDIX D: ENERGY SPREADING OF ORBIT IV

Here we show a series of snapshots of the vibration profile of the full system based on the MD simulations to demonstrate the energy spreading when the initial excitation is on orbit IV of the RS.

The results are shown in Fig. 11 for the excitation energy $E = 7.50$. It shows that the initial excitation energy flows rapidly to the other parts of the system in the form of a wave packet. The wavefront arrives at the boundaries at around $t \simeq 90$, and then due to the periodic boundary conditions, the system gradually steps into the equilibrium state. The long-lived DBs have not been observed during the MD simulations.

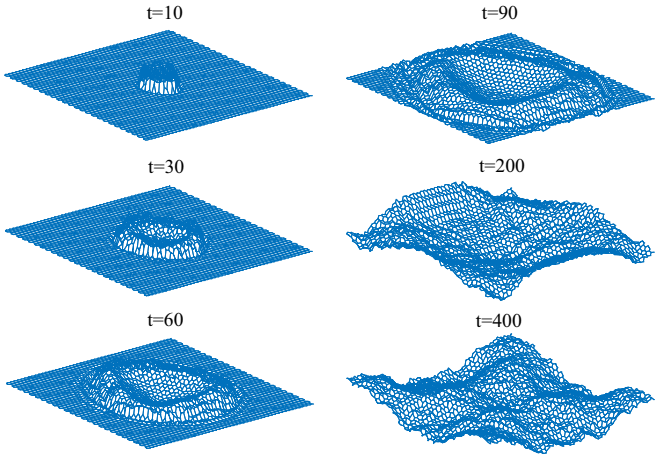

FIG. 11. The snapshots of the system when the initial condition is given by the orbit IV of the RS, and the excitation energy is $E = 7.50$.

[1] P. G. Kevrekidis, J. Cuevas-Maraver, and D. E. Pelinovsky, Energy Criterion for the Spectral Stability of Discrete Breathers, Phys. Rev. Lett. **117**, 094101 (2016).

[2] Y. Doi and K. Yoshimura, Symmetric Potential Lattice and Smooth Propagation of Tail-Free Discrete Breathers, Phys. Rev. Lett. **117**, 014101 (2016).

[3] N. Boechler, G. Theocharis, S. Job, G. P. Kevrekidis, A. M. Porter, and C. Daraio, Discrete Breathers in One-Dimensional Diatomic Granular Crystals, Phys. Rev. Lett. **104**, 244302 (2010).

[4] S. Flach, D. O. Krimer, and C. Skokos, Universal Spreading of Wave Packets in Disordered Nonlinear Systems, Phys. Rev. Lett. **102**, 024101 (2009).

[5] M. Sato and A. Sievers, Direct observation of the discrete character of intrinsic localized modes in an antiferromagnet, Nature (London) **432**, 486 (2004).

[6] M. E. Manley, O. Hellman, N. Shulumba, A. F. May, P. J. Stonaha, J. W. Lynn, V. O. Garlea, A. Alatas, R. P. Hermann, J. D. Budai, H. Wang, B. C. Sales, and A. J. Minnich, Intrinsic anharmonic localization in thermoelectric PbSe, Nat. Commun. **10**, 1928 (2019).

[7] V. S. Dmitriev, P. A. Chetverikov, and G. M. Velarde, Discrete breathers in 2D and 3D crystals, Phys. Status Solidi B **252**, 1682 (2015).

[8] D. Saadatmand, D. Xiong, V. A. Kuzkin, A. M. Krivtsov, A. V. Savin, and S. V. Dmitriev, Discrete breathers assist energy transfer to ac-driven nonlinear chains, Phys. Rev. E **97**, 022217 (2018).

[9] M. Sato, B. E. Hubbard, and A. J. Sievers, Colloquium: Nonlinear energy localization and its manipulation in micromechanical oscillator arrays, Rev. Mod. Phys. **78**, 137 (2006).

[10] S. Aubry, G. Kopidakis, and V. Kadelburg, Variational proof for hard discrete breathers in some classes of hamiltonian dynamical systems, Discrete Contin. Dyn. Syst., Ser. B **1**, 271 (2001).

[11] R. S. MacKay and S. Aubry, Proof of existence of breathers for time-reversible or hamiltonian networks of weakly coupled oscillators, Nonlinearity **7**, 1623 (1994).

[12] B. Gershgorin, Y. V. Lvov, and D. Cai, Renormalized Waves and Discrete Breathers in β-Fermi-Pasta-Ulam Chains, Phys. Rev. Lett. **95**, 264302 (2005).

[13] A. Lahiri, P. Majumdar, and A. Lahiri, Exact traveling breather solutions in a discrete Klein-Gordon ring, Phys. Rev. B **72**, 224306 (2005).

[14] J. C. Comte, Exact discrete breather compactons in nonlinear Klein-Gordon lattices, Phys. Rev. E **65**, 067601 (2002).

[15] A. V. Gorbach and M. Johansson, Discrete gap breathers in a diatomic Klein-Gordon chain: Stability and mobility, Phys. Rev. E **67**, 066608 (2003).

[16] C. Hoogeboom and P. G. Kevrekidis, Breathers in periodic granular chains with multiple band gaps, Phys. Rev. E **86**, 061305 (2012).

[17] C. Hoogeboom, P. G. Kevrekidis, A. Saxena, and A. R. Bishop, Discrete breathers in a nonlinear polarizability model of ferroelectrics, Phys. Rev. E **86**, 066601 (2012).

[18] O. V. Gendelman and L. I. Manevitch, Discrete breathers in vibroimpact chains: Analytic solutions, Phys. Rev. E **78**, 026609 (2008).

[19] B. Juanico, Y.-H. Sanejouand, F. Piazza, and P. DeLosRios, Discrete Breathers in Nonlinear Network Models of Proteins, Phys. Rev. Lett. **99**, 238104 (2007).

[20] Y. Zolotaryuk, S. Flach, and V. Fleurov, Discrete breathers in classical spin lattices, Phys. Rev. B **63**, 214422 (2001).

[21] L. Z. Khadeeva and S. V. Dmitriev, Discrete breathers in crystals with NaCl structure, Phys. Rev. B **81**, 214306 (2010).

[22] W. J. Fleischer, M. Segev, K. N. Efremidis, and N. D. Christodoulides, Observation of two-dimensional discrete solitons in optically induced nonlinear photonic lattices, Nature (London) **422**, 147 (2003).

[23] B. Eiermann, T. Anker, M. Albiez, M. Taglieber, P. Treutlein, K.-P. Marzlin, and M. K. Oberthaler, Bright Bose-Einstein Gap Solitons of Atoms with Repulsive Interaction, Phys. Rev. Lett. **92**, 230401 (2004).

[24] B. I. Swanson, J. A. Brozik, S. P. Love, G. F. Strouse, A. P. Shreve, A. R. Bishop, W.-Z. Wang, and M. I. Salkola, Observation of Intrinsically Localized Modes in a Discrete Low-Dimensional Material, Phys. Rev. Lett. **82**, 3288 (1999).

[25] L. Q. English, F. Palmero, P. Candiani, J. Cuevas, R. Carretero-González, P. G. Kevrekidis, and A. J. Sievers, Generation of Localized Modes in an Electrical Lattice using Subharmonic Driving, Phys. Rev. Lett. **108**, 084101 (2012).

[26] J. Cuevas, L. Q. English, P. G. Kevrekidis, and M. Anderson, Discrete Breathers in a Forced-Damped Array of Coupled Pendula: Modeling, Computation, and Experiment, Phys. Rev. Lett. **102**, 224101 (2009).

[27] N. Lazarides and G. P. Tsironis, Gain-Driven Discrete Breathers in $\mathcal{PT}$-Symmetric Nonlinear Metamaterials, Phys. Rev. Lett. **110**, 053901 (2013).

[28] S. Flach and C. R. Willis, Discrete breathers, Phys. Rep. **295**, 181 (1998).

[29] S. Flach and A. V. Gorbach, Discrete breathers advances in theory and applications, Phys. Rep. **467**, 1 (2008).

[30] S. Aubry, Discrete breathers: Localization and transfer of energy in discrete hamiltonian nonlinear systems, Physica D **216**, 1 (2006).

[31] Y. Y. Yamaguchi and Y. Doi, Low-frequency discrete breathers in long-range systems without on-site potential, Phys. Rev. E **97**, 062218 (2018).

[32] D. Xiong, Y. Zhang, and H. Zhao, Heat transport enhanced by optical phonons in one-dimensional anharmonic lattices with alternating bonds, Phys. Rev. E **88**, 052128 (2013).

[33] L. Z. Khadeeva and S. V. Dmitriev, Lifetime of gap discrete breathers in diatomic crystals at thermal equilibrium, Phys. Rev. B **84**, 144304 (2011).

[34] P. Maniadis, A. V. Zolotaryuk, and G. P. Tsironis, Existence and stability of discrete gap breathers in a diatomic β Fermi-Pasta-Ulam chain, Phys. Rev. E **67**, 046612 (2003).

[35] P. Maniadis and T. Bountis, Quasiperiodic and chaotic discrete breathers in a parametrically driven system without linear dispersion, Phys. Rev. E **73**, 046211 (2006).

[36] D. Hennig, Periodic, quasiperiodic, and chaotic localized solutions of a driven, damped nonlinear lattice, Phys. Rev. E **59**, 1637 (1999).

[37] C. Chong, P. G. Kevrekidis, G. Theocharis, and C. Daraio, Dark breathers in granular crystals, Phys. Rev. E **87**, 042202 (2013).

[38] B. Sánchez-Rey, G. James, J. Cuevas, and J. F. R. Archilla, Bright and dark breathers in Fermi-Pasta-Ulam lattices, Phys. Rev. B **70**, 014301 (2004).

[39] X.-L. Chen, S. Abdoulkary, P. G. Kevrekidis, and L. Q. English, Resonant localized modes in electrical lattices with second-neighbor coupling, Phys. Rev. E **98**, 052201 (2018).

[40] S. Flach, C. R. Willis, and E. Olbrich, Integrability and localized excitations in nonlinear discrete systems, Phys. Rev. E **49**, 836 (1994).

[41] S. Flach, K. Kladko, and C. R. Willis, Localized excitations in two-dimensional Hamiltonian lattices, Phys. Rev. E **50**, 2293 (1994).

[42] G. M. Chechin, S. V. Dmitriev, I. P. Lobzenko, and D. S. Ryabov, Properties of discrete breathers in graphane from *ab initio* simulations, Phys. Rev. B **90**, 045432 (2014).

[43] I. Evazzade, I. P. Lobzenko, E. A. Korznikova, I. A. Ovid'ko, M. R. Roknabadi, and S. V. Dmitriev, Energy transfer in strained graphene assisted by discrete breathers excited by external AC driving, Phys. Rev. B **95**, 035423 (2017).

[44] E. Barani, I. P. Lobzenko, E. A. Korznikova, E. G. Soboleva, S. V. Dmitriev, K. Zhou, and A. M. Marjaneh, Transverse discrete breathers in unstrained graphene, Eur. Phys. J. B **90**, 38 (2017).

[45] B. Liu, J. A. Baimova, S. V. Dmitriev, X. Wang, H. Zhu, and K. Zhou, Discrete breathers in hydrogenated graphene, J. Phys. D: Appl. Phys. **46**, 305302 (2013).

[46] L. Z. Khadeeva, S. V. Dmitriev, and Y. S. Kivshar, Discrete breathers in deformed graphene, JETP Lett. **94**, 539 (2011).

[47] Y. A. Baimova, S. V. Dmitriev, A. V. Savin, and Y. S. Kivshar, Velocities of sound and the densities of phonon states in a uniformly strained flat graphene sheet, Phys. Solid State **54**, 866 (2012).

[48] J. A. Baimova, R. T. Murzaev, and A. I. Rudskoy, Discrete breathers in graphane in thermal equilibrium, Phys. Lett. A **381**, 3049 (2017).

[49] K. A. Krylova, J. A. Baimova, R. T. Murzaev, and R. R. Mulyukov, Energy exchange between discrete breathers in graphane in thermal equilibrium, Phys. Lett. A **383**, 1583 (2019).

[50] G. Kopidakis and S. Aubry, Discrete breathers in realistic models: Hydrocarbon structures, Physica B **296**, 237 (2001).

[51] Y. Wang, Z. Zhu, Y. Zhang, and L. Huang, Metastable states and energy flow pathway in square graphene resonators, Phys. Rev. E **97**, 012143 (2018).

[52] C. Lobo and L. J. Martins, Valence force field model for graphene and fullerenes, Z. Phys. D **39**, 159 (1997).

[53] J. Atalaya, A. Isacsson, and M. J. Kinaret, Continuum elastic modeling of graphene resonators, Nano Lett. **8**, 4196 (2008).

[54] J. R. Chelikowsky and J. C. Phillips, Surface and thermodynamic interatomic force fields for silicon clusters and bulk phases, Phys. Rev. B **41**, 5735 (1990).

[55] A. Mehmood, N. Mubarak, M. Khalid, R. Walvekar, E. Abdullah, M. Siddiqui, H. A. Baloch, S. Nizamuddin, and S. Mazari, Graphene based nanomaterials for strain sensor application—A review, J. Environ. Chem. Eng. **8**, 103743 (2020).

[56] G. Yang, L. Li, W. B. Lee, and M. C. Ng, Structure of graphene and its disorders: A review, Sci. Technol. Adv. Mater. **19**, 613 (2018).

[57] D. J. Rizzo, G. Veber, T. Cao, C. Bronner, T. Chen, F. Zhao, H. Rodriguez, S. G. Louie, M. F. Crommie, and F. R. Fischer, Topological band engineering of graphene nanoribbons, Nature (London) **560**, 204 (2018).

[58] S. J. Bunch, M. v. d. A. Zande, S. S. Verbridge, W. I. Frank, M. D. Tanenbaum, M. J. Parpia, G. H. Craighead, and L. P. McEuen, Electromechanical resonators from graphene sheets, Science **315**, 490 (2007).

[59] G. Luo, Z. Zhang, G. Deng, H. Li, G. Cao, M. Xiao, G. Guo, L. Tian, and G. Guo, Strong indirect coupling between graphene-based mechanical resonators via a phonon cavity, Nat. Commun. **9**, 383 (2018).

[60] D. Midtvedt, A. Croy, A. Isacsson, Z. Qi, and H. S. Park, Fermi-Pasta-Ulam Physics with Nanomechanical Graphene Resonators: Intrinsic Relaxation and Thermalization from Flexural Mode Coupling, Phys. Rev. Lett. **112**, 145503 (2014).

[61] C. Chen, S. Rosenblatt, K. I. Bolotin, W. Kalb, P. Kim, I. Kymissis, H. L. Stormer, T. F. Heinz, and J. Hone, Performance of monolayer graphene nanomechanical resonators with electrical readout, Nat. Nanotech. **4**, 861 (2009).

[62] P. Weber, J. Gttinger, I. Tsioutsios, D. E. Chang, and A. Bachtold, Coupling graphene mechanical resonators to superconducting microwave cavities, Nano Lett. **14**, 2854 (2014).

[63] Y. Wang, Z. Zhu, Y. Zhang, and L. Huang, Symmetry blockade and its breakdown in energy equipartition of square graphene resonators, Appl. Phys. Lett. **112**, 111910 (2018).

[64] D. Davidovikj, F. Alijani, S. Cartamil-Bueno, H. van der Zant, M. Amabili, and P. Steeneken, Nonlinear dynamic characterization of two-dimensional materials, Nat. Commun. **8**, 1253 (2017).

[65] D. Song, F. Wang, G. Dukovic, M. Zheng, E. D. Semke, L. E. Brus, and T. F. Heinz, Direct Measurement of the Lifetime of Optical Phonons in Single-Walled Carbon Nanotubes, Phys. Rev. Lett. **100**, 225503 (2008).

[66] T. Shimada, D. Shirasaki, and T. Kitamura, Stone-Wales transformations triggered by intrinsic localized modes in carbon nanotubes, Phys. Rev. B **81**, 035401 (2010).

[67] R. Ishikawa, S. D. Findlay, T. Seki, G. Sánchez-Santolino, Y. Kohno, Y. Ikuhara, and N. Shibata, Direct electric field imaging of graphene defects, Nat. Commun. **9**, 1 (2018).